Journal of Nuclear Materials 380 (2008) 22–29

Contents lists available at ScienceDirect

Journal of Nuclear Materials

journal homepage: www.elsevier.com/locate/jnucmat

Clear band formation simulated by dislocation dynamics: Role of helical turns and pile-ups

Thomas Nogaret [a,b], David Rodney [a,*], Marc Fivel [a], Christian Robertson [b]

[a] SIMAP-GPM2, INP Grenoble, CNRS/UJF, BP46, 38402 Saint Martin d'Hères, France
[b] SRMA, CEA DEN/DMN Saclay, 91191 Gif-Sur-Yvette, France

ARTICLE INFO

Article history:
Received 4 July 2008
Accepted 11 July 2008

ABSTRACT

We present dislocation dynamics simulations of the glide of dislocations in random populations of Frank loops. Specific local rules of interaction are developed to reproduce elementary interaction mechanisms obtained from molecular dynamics simulations. We show that absorption of Frank loops as helical turns on screw dislocations is at the heart of the process of clear band formation because (1) it transforms the loops into jogs on dislocations, (2) when the dislocations unpin, the jogs are transported along the dislocation lines, leading to a progressive clearing of the band and (3) the dislocations are re-emitted in a glide plane different from the initial one, allowing for a broadening of the band. We also show that isolated dislocations cannot form a clear band of finite thickness because the clearing process would be limited to one plane tilted with respect to the {111} primary plane. Rather, a pile-up of dislocations is needed, leading to collective effects between dislocations that are analyzed in details.

1. Introduction

Neutron irradiation causes a degradation of the mechanical properties of metals that limit their lifetime in pressurized water reactors. A pronounced hardening, a ductility reduction and plastic instabilities are observed [1]. Hardening is due to the creation of a high density of nanometer-sized irradiation defect clusters that may be either of interstitial type, such as interstitial Frank Loops in stainless steel [2–4] or of vacancy type, such as stacking fault tetrahedra (SFT) in copper [5,6]. Ductility reduction and plastic instabilities are associated with the localization of the deformation in defect-free shear bands called 'clear bands' [7,8] where defects are removed by mobile dislocations during deformation. Clear bands are characterized by a constant thickness that depends on the resistance of the defects. Weaker defects, such as SFTs, lead to wider clear bands than stronger obstacles, such as Frank loops: ≈100 nm for the former compared to ≈20 nm for the latter [9]. The formation mechanism of clear bands remains however not well understood; namely, the clearing and broadening mechanisms of the bands are still unknown.

Recently, important modeling and experimental efforts have been devoted to investigate the elementary interaction mechanisms between dislocations and irradiations defects. Systematic studies were performed by molecular dynamics (MD) simulations [10,11]. The interaction mechanisms with Frank loops and SFTs were found in strong analogy. In both cases, edge and screw dislocations behave differently. Screw dislocations mainly absorb defects as helical turns whereas edge dislocations shear the defects at low applied stresses. Screw dislocations are strongly pinned by helical turns because the latter can glide only in the screw direction. When screw dislocations unpin, they are re-emitted in a glide plane parallel to the initial glide plane, because of the three-dimensional structure of the helical turn. Similar behaviors were observed in in situ transmission electron microscopy (TEM) [12]: screw dislocations are mainly responsible for defect removal, absorb defects as helical turns and are re-emitted in new glide planes upon unpinning. TEM observations showed also that clear bands are formed by screw dislocation pile-ups issued from heterogeneities, such as grain boundaries [8]. Conventional Frank Read sources are indeed strongly pinned by the formation of dense clouds of defects during the irradiation [13] and are inactive.

The efficiency of the above nano-scale interaction mechanisms in forming micron-scale clear bands has yet to be demonstrated. Dislocation dynamics (DD) simulations are suitable for addressing such a question. In the early 2000's, DD simulations were performed in order to study clear band formation by dislocations issued from a Frank Read source and interacting with a population of irradiation defects [14–17]. However the local rules used to model the short-range interactions between dislocations and irradiation defects were very simple: no distinction between screw and edge dislocation was made and the defects were systematically removed from the simulation cell after interaction.

In this paper, an existing DD code was modified to faithfully reproduce the MD interaction mechanisms. The different behaviors between screw and edge dislocations are reproduced with realism

* Corresponding author.
E-mail address: dvd.rodney@gmail.com (D. Rodney).

0022-3115/$ - see front matter © 2008 Elsevier B.V. All rights reserved.
doi:10.1016/j.jnucmat.2008.07.001

by using specific local rules of interaction and a undecorated dislocation source at a grain boundary is modeled. In Section 2, the simulation techniques are presented, i.e. the parameters and the configurations, the local rules of interaction and the elementary interaction mechanisms. In Section 3, the cases of a single edge or screw dislocation and of a screw dislocation pile-up in interaction with a random population of defects are presented. In Section 4, the results are discussed with respect to experiments and previous simulations.

2. The computational model

2.1. The simulation cell

We use the dislocation dynamics code developed by Verdier et al. which is described in details in Ref. [18]. We address here only the points specific to the present study. Dislocation lines are discretized in edge and screw segments that glide on a discrete lattice homothetic to the underlying crystallographic structure. Usually, the parameter of the discrete lattice is 10*b*, where *b* is the magnitude of the Burgers vector. In the present work, in order to model nanometric defects and subnanometric jogs on dislocations, we used a smaller parameter 0.08*b*. Consequently, we also used a smaller time step (5×10^{-14} s). Elasticity is isotropic and corresponds to a copper crystal in agreement with the MD simulations [11].

The simulation cell is shown in Fig. 1. Its dimensions are 0.6 μm × 0.6 μm × 0.24 μm. The borders act as impenetrable grain boundaries and cannot be crossed by the dislocations. Horizontal planes are $Z = (1\,1\,1)$ glide planes, while the Y axis is along the $[1\,0\,\bar{1}]$ Burgers vector direction. In order to account for dislocation emission from heterogeneities as observed experimentally in irradiated materials [8,22], we placed a dislocation source along a border of the cell, to model a grain boundary source. We tested different types of sources that emit either edge or screw dislocations as well as sources of different lengths (see Section 3.1). The applied stress tensor is composed of only the σ_{YZ} shear component which is controlled in order to impose a constant strain-rate $\dot{\epsilon}_{YZ} = 1.2 \times 10^3$ s^{-1}. No thermally-activated cross-slip is allowed.

In absence of detailed knowledge on how actual grain boundary sources operate, we used a simple emission criterion: the source emits a new dislocation when the applied stress σ_{YZ} reaches a critical value, called the *nucleation stress* τ_{nucl}. During a simulation, this stress is the maximum value that the applied stress may reach because in such a case, a dislocation is emitted, leading to an increment in plastic deformation that decreases the applied stress. The emitted dislocations belong to the $1/2\langle 1\,0\,\bar{1}\rangle\{1\,1\,1\}$ system, called primary system. The cross-slip system is $1/2\langle 10\bar{1}\rangle\{1\bar{1}1\}$. Both systems share the primary Burgers vector $1/2\langle 10\bar{1}\rangle$.

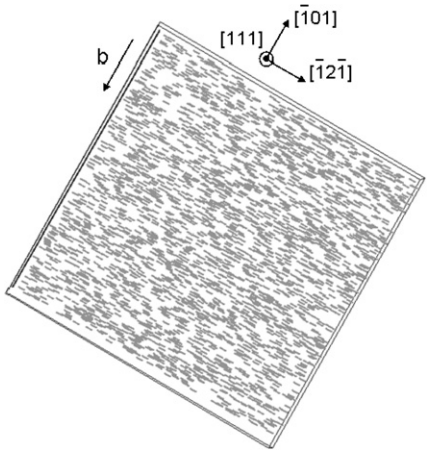

Fig. 1. Simulation cell. The loops are in grey, a screw dislocation appears in the upper left border.

The MD simulations show that when a Frank loop is unfaulted by interaction with a dislocation, it acquires systematically the Burgers vector of the dislocation [11]. Thus, in order to keep a simple computational model, we model the Frank loops as interstitial prismatic loops with the primary $1/2\langle 10\bar{1}\rangle$ Burgers vector. The initial loop shape is parallelepipedic, composed of 2 segments in the primary system and two segments in the cross-slip system. The length of the segments (and thus the loop size) is set to $D = 10$ nm. The loops are placed at random positions in the simulation cell, with a density $N = 3.7 \times 10^{22}$ m^{-3}, in agreement with typical TEM observations in irradiated stainless steels [4]. The mean inter-loop distance in glide planes is then $L = 1/\sqrt{N \times D} = 52$ nm, which corresponds to the distance considered in the MD simulations.

2.2. Elementary interaction mechanisms

Frank loops are sessile because of their stacking fault. They are unfaulted and become glissile through the interaction with screw dislocations, while they remain faulted and are only sheared when interacting with edge dislocations. In order to reproduce these elementary interactions, the loops in the simulation cell are initially '*frozen*', i.e. their segments are immobile. When a dislocation meets a loop, its character is identified by computing the angle between the local tangent to the dislocation line and the Burgers vector. If this angle is ±20°, the dislocation is declared screw and the loop segments are '*freed*', i.e. they are allowed to move according to the forces acting on them. As will be seen in next paragraph, a helical turn then forms spontaneously. If the dislocation is not screw, the loop remains '*frozen*' and the contacting dislocation segments cannot react with the loop. The dislocation is allowed to cross the loop when its arms on both sides of the loop reach a critical angle that was set to 100° in order to match the resistance obtained in MD simulations, i.e. a critical shear stress of 130 MPa for an inter-loop distance of 50 nm [11].

The interaction between a screw dislocation and Frank loops is illustrated in Fig. 2. The dislocation is 200 nm long and is pinned at both ends. The inter-loop distance is 50 nm (Fig. 2(a)). When an increasing shear stress is applied, the dislocation bows out and contacts the central Frank loop with a screw character. The segments forming the loop are thus freed. They react with the dislocation and form spontaneously a helical turn (Fig. 2(b)). The latter consists of 20-nm long segments: 3 super-jogs in $(1\bar{1}1)$ cross-slip planes and 2 segments in $(1\,1\,1)$ primary planes located above and below the initial glide plane. As the stress is increased, the dislocation advances, meets the other loops and absorbs them as two additional helical turns (Fig. 2(c)). The dislocation ends up with a 3D structure. It does not belong to the initial glide plane anymore because the helical turns expanded along the dislocation line in order to minimize the dislocation length and the associated line tension energy. The dislocation is pinned by the helical turns because the super-jogs in cross-slip planes can glide only in the $[10\bar{1}]$ direction of the Burgers vector, i.e. along the dislocation line, and not in the $[\bar{1}2\bar{1}]$ glide direction. Dislocation unpinning requires the activation of a 20 nm long super-jog in a $(1\,1\,1)$ glide plane (Fig. 2(d)), requiring a high applied stress of 340 MPa. The activated segment belongs to a $(1\,1\,1)$ plane located above (along the $[1\,1\,1]$ direction) the initial glide plane. Indeed, it can be shown from a line tension approximation of a helical turn that upon increasing shear stress, the segment located furthest in the glide direction becomes unstable first. Consequently, a dislocation that glides in the $[\bar{1}2\bar{1}]$ (resp. $[1\bar{2}1]$) direction is re-emitted in an upper (resp.

Fig. 2. Interaction between a screw dislocation and Frank loops. (a) 60 MPa, 95 ps: the dislocation glides in a (1 1 1) plane intersecting the loops in their middle; (b) 60 MPa, 155 ps: the dislocation comes into contact with the central loop that is absorbed as a helical turn; (c) 60 MPa, 300 ps: the three loops are absorbed as helical turns; (d) 340 MPa, 680 ps: a dislocation segment located in an upper (1 1 1) plane is activated and pushes the super-jogs on the sides.

lower) (1 1 1) plane. We will see in the following that this unpinning mechanism plays a central role in clear band broadening. As the activated segment bows out, it pushes the super-jogs towards the cell borders (Fig. 2(d)). After unpinning, glissile loops are left behind, located on either sides of the dislocation. We will see that this '*pushing*' mechanism is central to band clearing.

The interaction between an edge dislocation and 3 Frank loops is illustrated in Fig. 3. As a stress is applied, the dislocation bows out and comes into contact with the loops with an edge character (Fig. 3(b)). The dislocation is blocked and bows out. When the stress reaches 130 MPa, the angle between the dislocation arms pinned on the central loop reaches the critical angle of 100° (Fig. 3(c)) and the dislocation is allowed to go through the loop. The latter remains '*frozen*' and is left unchanged, since it was observed in MD simulations that the step created on the loop is mobile and annihilates on the loop border, thus reforming the initial loop configuration.

3. Glide in random loop environments

In this section, the glide of dislocation(s) through a random population of Frank loops is simulated. Two glide regimes are studied by changing the magnitude of the nucleation stress τ_{nuc}. We consider first the case where the nucleation stress is much larger than the loop resistance evaluated in Section 2.2. A single dislocation then glides through the simulation cell, pushed only by the applied stress. In the second regime, the nucleation stress is lower than the loop resistance. A single dislocation cannot glide on its own. Multiple dislocations are then nucleated and form a pile-up, leading to collective interaction effects that enable the dislocations

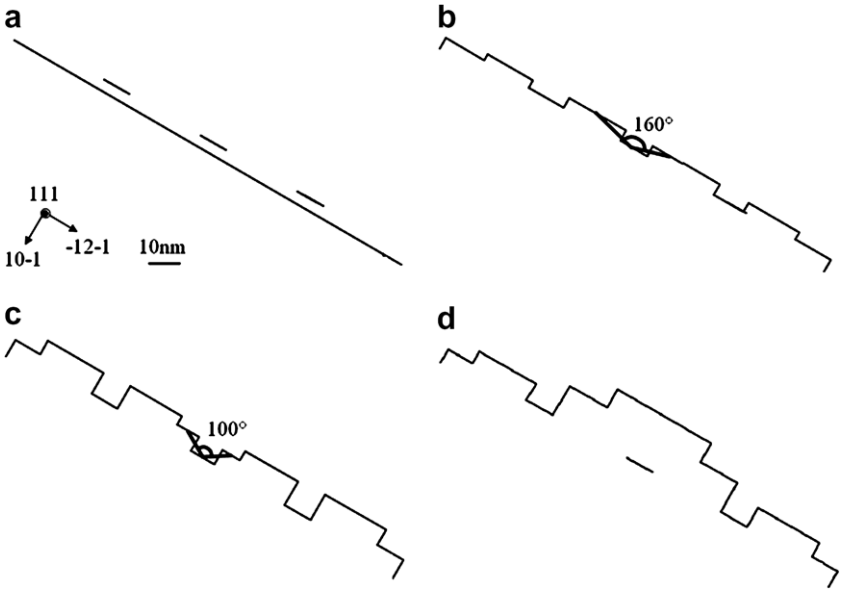

Fig. 3. Interaction between an edge dislocation and Frank loops. (a) 0 MPa, 0 ps: initial configuration; (b) 67 MPa, 22 ps: the dislocation is blocked by the loops; (c) 125 MPa, 39 ps: the critical bowing angle of 100° is reached on the central loop; (d) 130 MPa, 44 ps: the dislocation has crossed the central loop that remains 'frozen'.

to glide through the cell at an applied stress lower than when isolated.

3.1. Glide of single dislocations

We used a nucleation stress of 1000 MPa, much larger than the loop resistance evaluated in previous Section. The applied stress needed to accommodate the imposed plastic strain rate then never reaches the nucleation stress and only one dislocation glides through the cell. We study here dislocation sources that emit 200 nm long dislocations of either edge or screw character.

Let's consider first the case of an edge source, as shown in Fig. 4. In Fig. 4(a) which shows a [1 1 1] top view of the simulation cell, we see that the edge part emitted from the source glides mainly by shearing loops. It produces on its sides two long dislocations of screw character. The latter are wavy and composed of segments in the primary glide plane as well as in cross-slip planes. These segments form helical turns created on the dislocation line by the unfaulting and absorption of Frank loops, following the same interaction mechanism as described in Section 2.2. While the edge segment is mobile, the two screw dislocations are strongly pinned. The $[1\bar{2}1]$ side view of Fig. 4(c) shows that dislocation glide is planar on average, although segments in cross-slip planes, that belong to helical turns, are also visible. The stress/strain curve in Fig. 4(b) shows that the stress required for the glide of a single edge dislocation is between 130 and 160 MPa, depending on the local loop density met by the dislocation along its path.

The screw case is shown in Fig. 5. As the screw dislocation emitted from the source advances through the simulation cell, it creates edge parts that glide easily until they reach the cell borders, while the screw segment unfaults and absorbs loops as helical turns (see Fig. 5(a)). The dislocation soon adopts the shape of a long screw segment that traverses the whole cell in the $[10\bar{1}]$ direction, with edge segments stacked on the cell boundaries. Thus, edge and screw sources lead to similar microstructures made of screw dislocations that extend over the entire length of the simulation cell.

With the screw source, the stress required for dislocation glide is between 200 and 260 MPa, as seen on the stress/strain curve of Fig. 5(b). The screw dislocation advances through the simulation cell by a mechanism close to the elementary mechanism described in Section 2.2: a succession of formation of helical turns that pin the dislocation followed by the activation of segments in the

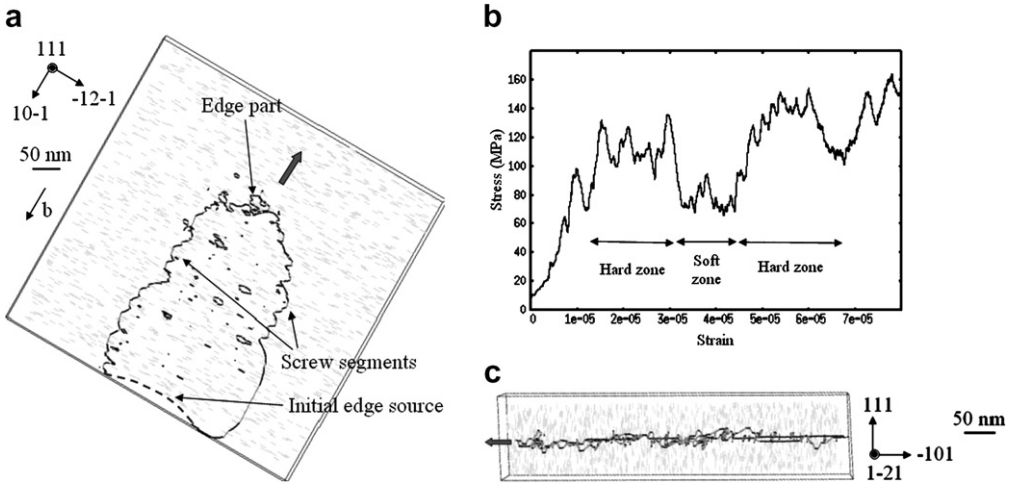

Fig. 4. Glide of a single edge dislocation: (a) [1 1 1] top view (untouched loops are in light grey, segments in (1 1 1) planes in blue, segments in cross-slip planes in orange), (b) stress/strain curve, (c) $[1\bar{2}1]$ side view (the green arrow shows the direction of glide). (For interpretation of the references to colour in this figure legend, the reader is referred to the web version of this article.)

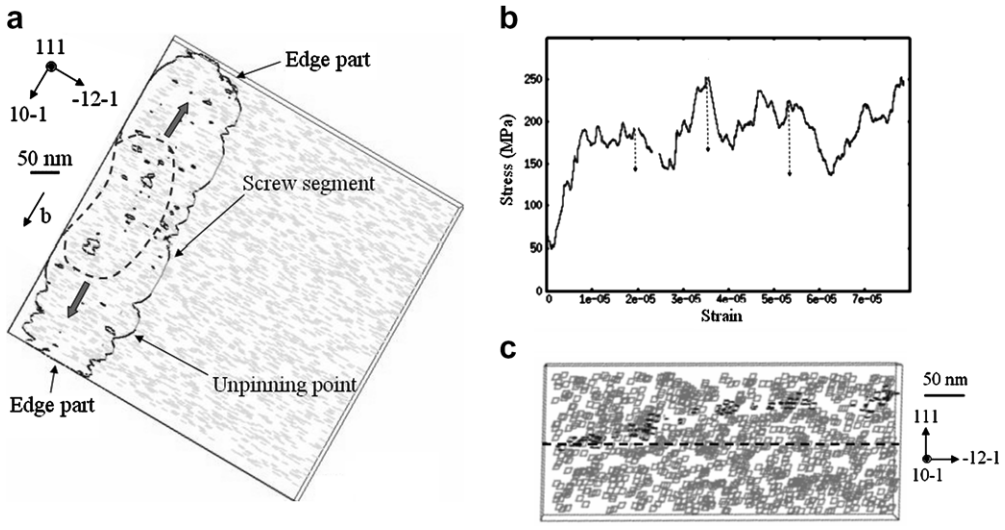

Fig. 5. Glide of a single screw dislocation: (a) [1 1 1] top view, (b) stress/strain curve, (c) $[10\bar{1}]$ side view on a 200 nm thick thin foil.

weakest zones along the dislocation, i.e. the zones where the jog density is the lowest. The activated segments glide on about 100 nm before being pinned again by helical turns. During this process, edge segments are created and glide easily towards the cell borders. Each activation event induces a stress drop indicated by arrows on the stress/strain curve in Fig. 5(b). The edge segments, while travelling towards the cell borders, sweep the dislocation line and push the jogs on a finite distance towards the cell borders. This mechanism allows for a partial and progressive clearing of the swept zone.

As in the elementary reactions, when the screw dislocation unpins, it is systematically re-emitted in an upper (1 1 1) plane. Consequently, as seen in the $[10\bar{1}]$ side view in Fig. 5(c), the dislocation glides in an average non-crystallographic plane, inclined with respect to the initial (1 1 1) plane, in contradiction with experimental observations. Moreover, no clearing is observed in Fig. 5(c).

We have seen that plasticity is limited by screw dislocations and that both edge and screw dislocation sources lead to the same anisotropic microstructure with strongly pinned screw segments that extend over the entire length of the simulation cell. Thus in the following, we will consider only the case of a screw dislocation source with a length equal to that of the simulation cell.

3.2. Collective dislocation motion

Now, in contrast with previous simulations, we consider a low nucleation stress of 90 MPa, below the critical stress for edge or screw dislocation glide. Consequently, a single dislocation cannot glide on its own, and collective effects are needed to keep on deforming the simulation cell at the prescribed strain rate. Fig. 6 illustrates the glide mechanism. The first dislocation nucleated acquires helical turns as in previous Section and gets pinned. The stress in the cell increases and reaches the nucleation stress, as shown by an arrow in Fig. 6(b). A second dislocation is then nucleated. It produces some plastic strain, allowing the applied stress to drop. This second dislocation gets also pinned, and the applied stress rises again, triggering the nucleation of a third dislocation, materialized by another arrow in Fig. 6(b). A pile-up, clearly visible in Fig. 6(a), thus forms progressively. It advances in the cell thanks to collective effects that include a stress concentration due to the pile-up effect, short-range interaction mechanisms (arm exchange) and avalanches of dislocation glide. The collective effects are detailed in next paragraph. But before, note that the pile-up displays a specific structure. The four leading dislocations are wavy and heavily jogged. They are responsible for clearing the band by forming helical turns and pushing the jogs towards the cell borders upon unpinning. Accumulation of jogs are visible on the sides of the cell in Fig. 6(a). Trailing dislocations contain very few jogs because they glide in the region cleared by the leading dislocations. The role of the trailing dislocations is to produce the pile-up effect and to concentrate the stress on the leading dislocations. Some heavily jogged dislocations are left behind, as seen in Fig. 6(a). They will presumably remain in the clear band. As in previous Section, the leading dislocations unpin in upper (1 1 1) planes and remain pushed by the pile-up effect as long as they are not too far away from the initial central glide plane. As a consequence, as seen in Fig. 6(c), a cleared region of finite thickness develops parallel to the central (1 1 1) glide plane, in agreement with experiments.

We now detail the three collective effects that allow for dislocation glide. A first effect is the classic pile-up effect. The stress ahead of the pile-up is concentrated, providing the additional stress necessary to reach the unpinning stress: $\tau_{\text{unpinning}} = \tau_{\text{applied}} + \tau_{\text{pile-up}}$ with $\tau_{\text{pile-up}} \propto N_{\text{dislocation}} \cdot \tau_{\text{applied}}$ for an ideal pile-up of rectilinear infinite dislocations [19].

However, dislocations in presence of Frank loops are not rectilinear but jogged because of the helical turns and do not belong to the central glide plane. This reduces the stress created by the pile-up as illustrated in Fig. 7(a). The latter shows the resolved shear stress created by a screw dislocation (D2) either rectilinear or jogged on another screw dislocation. The jogged dislocation was obtained using the superposition shown in Fig. 7(b) where the stress field of the loops was calculated from the expressions derived in Ref. [20]. The resolved shear stress produced by the jogged dislocation is lower than that produced by the rectilinear dislocation. It tends to zero when the distance between dislocations tends to zero. The reason is that the shear stress produced by the loops is zero in the central glide plane such that the stress produced by the jogged dislocation is proportional to $r/(r^2 + R_{\text{loop}}^2)$, rather than $1/r$ (r is the distance between dislocations and R_{loop} is the size of the loops, 10 nm in the present case). Note also that since the stress produced by the jogged dislocation remains finite at short distance, the jogged and rectilinear dislocations can come into contact, leading to contact interactions described in the next paragraph.

A second collective effect is an 'arm exchange', as already observed in MD simulations [11] and experiments [12]. Arm exchanges lower the resistance on the dislocation lines because

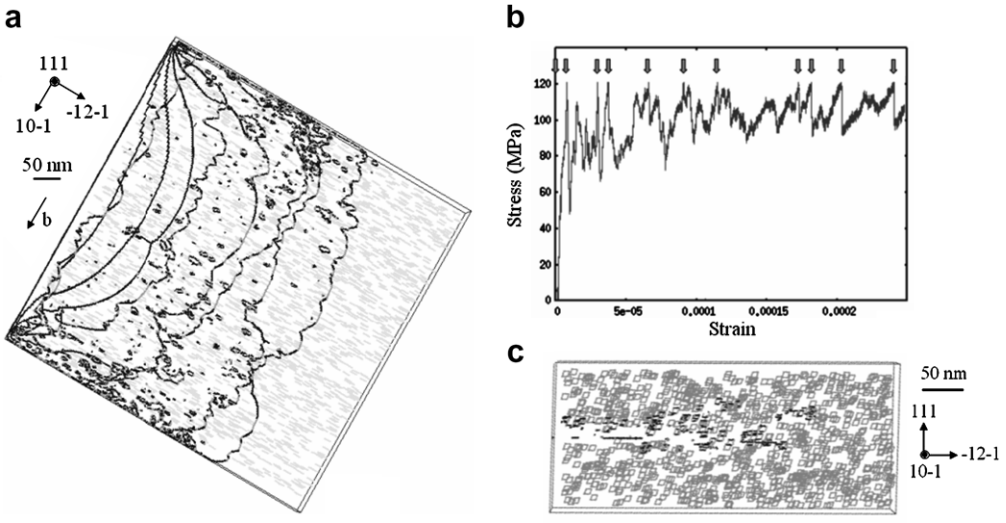

Fig. 6. Glide of a dislocation pile-up: (a) [1 1 1] top view, (b) stress/strain curve, (c) $[10\bar{1}]$ side view on a 200 nm thick thin foil.

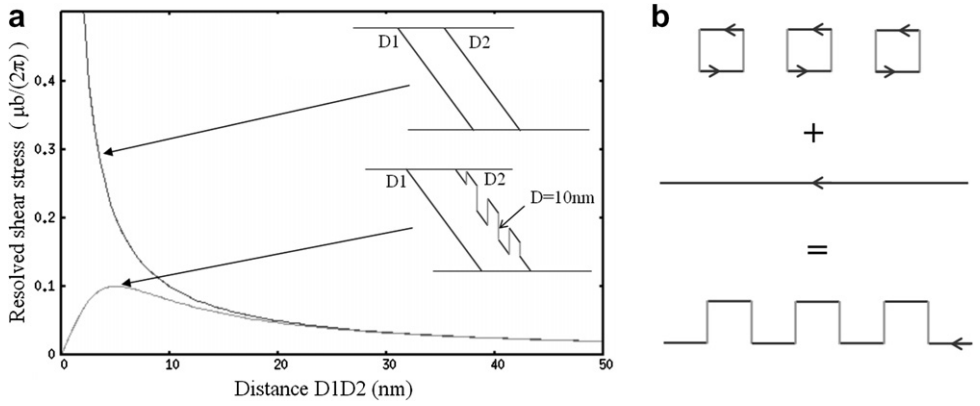

Fig. 7. Screening by helical turns of interaction between dislocations. (a) Resolved shear stress as a function of distance between a rectilinear screw dislocation and either a rectilinear or a jogged screw dislocation. (b) Decomposition of a jogged dislocation into a regular array of loops and a rectilinear screw dislocation.

they permit to decrease locally the jog density by sharing jogs between a heavily jogged leading dislocation and a weakly jogged trailing dislocation. Two examples of arm exchange are shown in Figs. 8 and 9, the former being temporary, the latter permanent.

A temporary arm exchange is shown Fig. 8. A weakly jogged dislocation D2 comes into contact with a heavily jogged dislocation D1 (Fig. 8(a)). An arm exchange occurs in Fig. 8(b) whereby the left part L1 of D1 reconnects with the right part R2 of D2, while the right part R1 of D1 reconnects with the left part L2 of D2. Two composite dislocations are thus formed: L1R2 and L2R1. Jogs are then transferred from L1 to R2, locally decreasing the jog density and the corresponding glide resistance. As a consequence, the segment marked by an arrow in Fig. 8(c) gets activated and R1 to recombine with L1 to reform the initial dislocation D1 (Fig. 8(d)), which can now glide over some distance before reforming another helical turn.

A permanent arm exchange is depicted in Fig. 9. Dislocation D2 (L2C2R2) is weakly jogged and glides in the central plane whereas dislocation D1 (L1C1R1) is heavily jogged and has its central part C1 in an upper glide plane (Fig. 9(a)). Segment C2 reconnects with L1 while L2 reconnects with C1 (Fig. 9(b)). Then, C2 reconnects with R1 and R2 reconnects with C1, thus forming two composite dislocations (L1C2R1) and (L2C1R2) (Fig. 9(c)). The result is that the unjogged segment C2 can glide further.

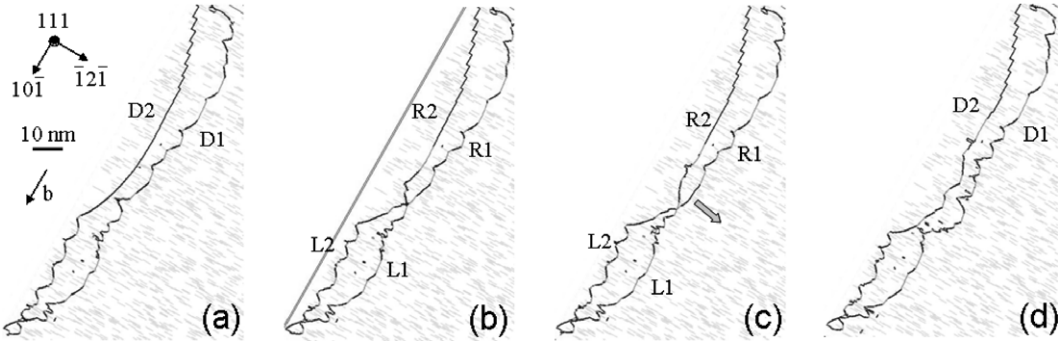

Fig. 8. Temporary arm exchange, [1 1 1] views: see text for details.

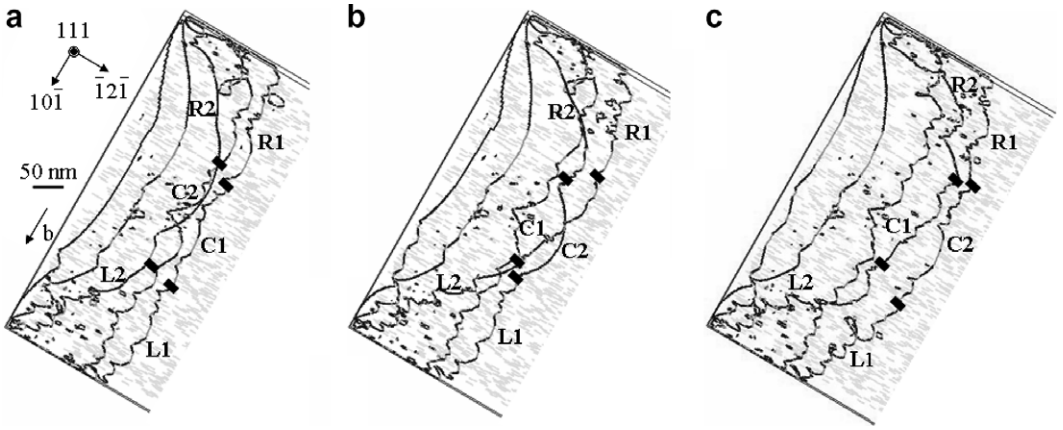

Fig. 9. Permanent arm exchange, [1 1 1] views: see text for details.

A third collective effect is an avalanche effect: the activation of a segment on a dislocation in a pile-up can activate segments on its preceding and following dislocations that can also activate segments on their neighboring dislocations, and so on, inducing an avalanche of activations. Avalanches result from two mechanisms. First, when a segment is activated, it pushes the jogs towards its sides, forming a long dislocation segment without jogs that pushes more efficiently the dislocations ahead of it (increasing of the pile-up effect described above), thus favoring their unpinning. Second, when a dislocation segment in a pile-up unpins, it advances and its repulsive elastic field on the dislocations located behind it decreases, facilitating their activation.

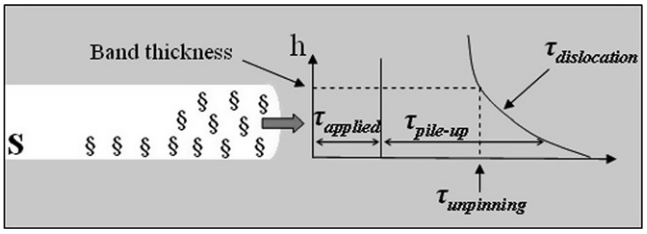

Fig. 10. Schematic representation of the equilibrium between the stress on the dislocations $\tau_{dislocation}$ (equal to the sum of the applied stress $\tau_{applied}$ and the pile-up stress concentration $\tau_{pile\text{-}up}$) and the defect resistance $\tau_{unpinning}$, which sets the band thickness.

4. Discussion

For the present study, we adapted dislocation dynamics to the nanometer scale in order to reproduce with realism the elementary interaction mechanisms observed in MD simulations. As a consequence, the computation load becomes very large and only the first stage of the clear band formation was simulated (see Fig. 6(c)) in a small grain. However, this study allows us to draw some conclusions about the mechanisms at the heart of the process.

The simulations confirm earlier MD results on the central role played by helical turns in clear band formation. Screw dislocations transform Frank loops into helical turns. The helical turns are then transported along the dislocation lines when they unpin leading to a progressive clearing of the band and to the accumulation of jogs and prismatic loops aligned in the edge direction. These loops have the same Burgers vector as the emitted dislocations, i.e. the primary Burgers vector. Helical turns are also central to clear band widening because upon unpinning, screw dislocations are re-emitted in new glide planes. This is equivalent to a double cross-slip over a height set by the loop size. This mechanism is consistent with the work of Neuhauser and Rodloff [21] who observed on the surface of irradiated and deformed copper a distance between slip lines on the order to the defect size. Note that all the effects observed in the simulations were obtained while thermally-activated cross-slip and climb were switched-off. Thus, thermal activation is not a necessary condition for clear band formation.

The microstructure obtained in the simulations, composed of long screw dislocations with accumulations of jogs and prismatic loops on the sides, is consistent with the TEM observations made by Sharp [7] who reported inside clear bands the presence of dense clusters of heavily jogged prismatic loops with a low density of screw dislocations, all sharing the same Burgers vector. To our knowledge, Sharp's work is the only case where a thin foil was prepared parallel to a clear band, making possible a detailed analysis of the microstructure *inside* a clear band. All other TEM studies of clear bands in irradiated materials used thin foils perpendicular to the clear band, which is the best orientation to locate a clear band, but the worst to study the microstructure inside the band. The reason is twofold. First, when the foil is perpendicular to the band, the depth of the band is minimum (equal to the depth of the thin foil) and only very few defects may be present in the band. For example, in Sharp's study, the distance between loop clusters is 0.5 μm, larger than the typical thin foil depth (0.1 μm). Second, when the foil is perpendicular to the band, the $g \cdot b = 0$ condition is satisfied for the dislocations with a Burgers vector parallel to the band. In this condition, the contrast on the dislocations and the prismatic loops (that share the primary Burgers vector) is minimum.

The present work shows the central role played by dislocation pile-ups. Isolated dislocations can not form clear bands because clearing is very progressive. Also, isolated screw dislocations glide on non-crystallographic planes, owing to their systematic re-emission in upper (1 1 1) planes (see Fig. 5(c)). By way of contrast, when dislocations glide in pile-up, they remain along the central (1 1 1) plane (see Fig. 6(c)) and they clear the band more efficiently. Sources of dislocations at the origin of clear bands must therefore emit a large number of dislocations. Since the sources prior to the irradiation are locked by decoration, the most probable sources are grain boundaries or other stress concentrators, such as inclusions [22]. Clearly, more atomistic insights are needed to better understand how heterogeneities may act as dislocation sources and in absence of this knowledge, we used a very simplified criterion. Note that hardening is not described in the present simulations because the resistance of the source, which controls the flow stress, is given as preset parameter.

We have not been able to study in details what controls the width of the clear bands because the simulation times were too long. However, one possible origin is the decay of the stress concentration away from the plane of the pile-up. Indeed, the leading dislocations of the pile-ups are heavily jogged and need a stress concentration to advance in the cell. As illustrated in Fig. 10, the stress on the dislocations ($\tau_{dislocation}$) is the sum of the applied stress ($\tau_{applied}$) and the stress concentrated by the pile-up ($\tau_{pile\text{-}up}$). The former is constant inside the simulation cell while the latter decreases away from the plane of the pile-up. When the leading dislocations unpin and are re-emitted in upper glide planes, they are subjected to a decreasing stress. There is thus a critical distance from the pile-up plane, which sets the band thickness, where the stress on the dislocations just balances the resistance due to the helical turns ($\tau_{unpinning}$) and the dislocations stop. In their displacement, the leading dislocations have started to clear the band and the trailing dislocations can move forward and themselves glide away from the plane of the pile-up until they are stopped and so on. This scenario should be confirmed by longer simulations. It predicts that heavily jogged screw dislocations should be left in the upper plane of the clear band. Although such arrays of screw dislocations have been observed [8], more TEM studies are needed. The present scenario also explains the experimental observation that the band width decreases when the resistance of defects or the resolved shear stress [9] or the defect density [7] increase. Indeed, for a given size of pile-up, the band width decreases if $\tau_{unpinning}$ increases, i.e. if the defects are intrinsically stronger or if they are in higher density; it also decreases if the resolved shear stress ($\tau_{applied}$) decreases.

5. Conclusion

The present work concludes a multiscale simulation study of the formation of clear bands. An existing DD code was modified to reproduce accurately MD results on elementary interaction mechanisms at the nanometer scale. The DD simulations in random loop environments confirm the central role played by helical turns in the formation of clear bands. It also shows that clear bands can not form without dislocation pile-ups. From the simulations,

we predict that well-developed clear bands should contain heavily jogged screw dislocations as well as dense concentrations of prismatic loops. In order to confirm these predictions, detailed TEM analysis of the dislocation microstructure *inside* clear bands are needed.

Acknowledgement

This work was funded by the European PERFECT Project (No. FI60-CT-2003-508840).

References

[1] K. Farrell, T. Byun, N. Hashimoto, J. Nucl. Mater. 335 (2004) 471.
[2] M. Suzuki, A. Sato, N. Nagakawa, H. Shiraishi, Phil. Mag. A 65 (1992) 1309.
[3] Y. Dai, X. Jia, J. Chen, W. Sommer, M. Victoria, G. Bauer, J. Nucl. Mater. 296 (2001) 174.
[4] C. Pokor, Y. Bréchet, P. Dubuisson, J. Massoud, A. Barbu, J. Nucl. Mater. 326 (2004) 19.
[5] B. Singh, S. Zinkle, J. Nucl. Mater. 206 (1993) 212.
[6] M. Victoria, N. Baluc, C. Bailat, Y. Dai, M. Luppo, R. Schaublin, J. Nucl. Mater. 276 (2000) 114.
[7] J. Sharp, Philos. Mag. 16 (1967) 77.
[8] J. Robach, I. Robertson, A. Arsenlis, Philos. Mag. 83 (2003) 955.
[9] N. Hashimoto, T. Byun, K. Farrell, J. Nucl. Mater. 351 (2006) 295.
[10] Y. Osetsky, D. Rodney, D. Bacon, Philos. Mag. 86 (2006) 2295.
[11] T. Nogaret, C. Robertson, D. Rodney, Philos. Mag. 87 (6) (2007) 945.
[12] Y. Mastukawa, Y. Osetsky, R. Stoller, S. Zinkle, Philos. Mag. 88 (2008) 581.
[13] B. Singh, A. Foreman, H. Trinkaus, J. Nucl. Mater. 249 (1997) 103.
[14] T. delaRubia, H. Zbib, T. Khraishi, B. Wirth, M. Victoria, M. Caturla, Nature 406 (2000) 871.
[15] N. Ghoniem, S. Tong, B. Singh, L. Sun, Philos. Mag. A 81 (2001) 2743.
[16] T. Khraishi, H. Zbib, T. de la Rubia, M. Victoria, Met. Mat. Trans. B 33 (2002) 285.
[17] N. Ghoniem, S. Tong, J. Huang, B. Singh, M. Wen, J. Nucl. Mater. 307–311 (2002) 843.
[18] M. Verdier, M. Fivel, I. Groma, Mod. Sim. Mater. Sci. Eng. 6 (1998) 755.
[19] J.P. Hirth, J. Lothe, Theory of Dislocations, Krieger, Malabar, 1992.
[20] T. Khraishi, H. Zbib, Philos. Mag. Lett. 82 (2002) 265.
[21] H. Neuhauser, R. Rodloff, Acta Metal. 22 (1974) 375.
[22] D. Edwards, B. Singh, J. Bilde-Sorensen, J. Nucl. Mater. 342 (2005) 164.